

See discussions, stats, and author profiles for this publication at: <https://www.researchgate.net/publication/45287944>

Tailored Au nanorods: Optimizing functionality, controlling the aspect ratio and increasing biocompatibility

Article in *Nanotechnology* · August 2010

DOI: 10.1088/0957-4484/21/33/335604 · Source: PubMed

CITATIONS

21

READS

498

11 authors, including:



Xiaoqing Cai

Shanghai Institute of Applied Physics

19 PUBLICATIONS 614 CITATIONS

[SEE PROFILE](#)



Hsianghsin Chen

Academia Sinica

51 PUBLICATIONS 632 CITATIONS

[SEE PROFILE](#)



Chia-Chi Chien

University of South Australia

46 PUBLICATIONS 891 CITATIONS

[SEE PROFILE](#)



Sheng-Feng Lai

Academia Sinica

29 PUBLICATIONS 296 CITATIONS

[SEE PROFILE](#)

Some of the authors of this publication are also working on these related projects:



Mechanism of lung diseases [View project](#)



Electronic Structure of High Temperature Superconductors [View project](#)

Tailored Au nanorods: optimizing functionality, controlling the aspect ratio and increasing biocompatibility

This article has been downloaded from IOPscience. Please scroll down to see the full text article.

2010 Nanotechnology 21 335604

(<http://iopscience.iop.org/0957-4484/21/33/335604>)

View [the table of contents for this issue](#), or go to the [journal homepage](#) for more

Download details:

IP Address: 140.109.101.40

The article was downloaded on 27/07/2010 at 13:29

Please note that [terms and conditions apply](#).

Tailored Au nanorods: optimizing functionality, controlling the aspect ratio and increasing biocompatibility

Xiaoqing Cai¹, Cheng-Liang Wang¹, Hsiang-Hsin Chen¹,
Chia-Chi Chien^{1,2}, Sheng-Feng Lai¹, Yi-Yun Chen¹, Tzu-En Hua¹,
Ivan M Kempson¹, Y Hwu^{1,2,3,6}, C S Yang⁴ and G Margaritondo⁵

¹ Institute of Physics, Academia Sinica, Nankang, Taipei 115, Taiwan

² Department of Engineering and System Science, National Tsing Hua University, Hsinchu 300, Taiwan

³ Institute of Optoelectronic Sciences, National Taiwan Ocean University, Keelung 202, Taiwan

⁴ Center for Nanomedicine, National Health Research Institutes, Miaoli, Taiwan

⁵ Ecole Polytechnique Fédérale de Lausanne (EPFL), CH-1015 Lausanne, Switzerland

E-mail: pwhwu@sinica.edu.tw

Received 4 April 2010, in final form 5 July 2010

Published 26 July 2010

Online at stacks.iop.org/Nano/21/335604

Abstract

Monodisperse gold nanorods with high aspect ratio were synthesized by x-ray irradiation. Irradiation was first used to stimulate the creation of seeds. Afterward, nanorod growth was stimulated either by chemical reduction or again by x-ray irradiation. In the last case, the entire process took place without reducing agents. The shape of the final products could be controlled by modulating the intensity of the x-ray irradiation during the seed synthesis. In turn, the nanorod aspect ratio determines the absorption wavelength of the nanorods that can thus be optimized for different applications. Likewise, the aspect ratio influences the uptake of the nanorods by HeLa cells.

(Some figures in this article are in colour only in the electronic version)

1. Introduction

Intense x-ray irradiation was recently used to stimulate the synthesis of nanoparticles producing highly stable and clean nanosols [1–4]. The combination of high intensity and deep penetration leads to fast reduction and particle nucleation throughout the solution. We repeatedly tried to extend this method to the synthesis of nanorods but such attempts were so far unsuccessful.

Here we report on the solution to this problem: by tuning the irradiation intensity, we could not only grow nanorods but also gain full control of their geometric characteristics. This solution still provides all the advantages of irradiation-induced nanoparticle synthesis (including the possibility

of *in situ* monitoring by x-ray techniques) and therefore constitutes a significant step in nanofabrication.

Nanorod fabrication is one example of the exploitation of the dependence of nanoparticle characteristics on the size, shape and surface properties [5]. Nanorods are potentially interesting for applications in nanotechnology and nanomedicine. For example, as their aspect ratio increases their optical absorption shifts towards the infrared [6]. Optimizing absorption while matching the spectral windows for transmission in animal tissues therefore enhances the possible use of the nanorods for cancer detection, thermal treatment and other nanomedicine applications [6–15]. As a consequence, several nanorod synthesis approaches have been developed in recent years, such as templating [16], photochemistry [17, 18], electrochemistry [19] and seeded growth methods in aqueous solution [20–22]. Among these, the seeded growth methods are quite effective for

⁶ Address for correspondence: Institute of Physics, Academia Sinica, Taipei 11529, Taiwan.

the control of size and shape. Irradiation-based approaches could further improve the seeding methods by altogether eliminating the need for reducing agents and the corresponding complications [23].

In this instance, free radicals are directly produced by the interaction of the irradiating photons with the solvent and cause reduction without additional reagents. The reduction can thus be controlled, e.g., by adjusting the irradiating beam intensity. The control is produced by physical rather than chemical factors with considerable advantages: for example, the reaction can be switched on or off instantaneously, or simply and quickly adjusted to a desired rate without dealing with reagents, surfactants and stabilizers. This flexible control is particularly attractive for the synthesis of nanoparticles.

Irradiation-induced synthesis was indeed already used to nucleate nanoparticles from solution [1–4, 24–27]. However, reducing agents were still used while irradiating with low-intensity γ -rays [24], or required very long exposure times—up to tens of hours with electrons [25] or x-rays [26, 27]. Prolonged irradiation leads to colloidal stability problems in these synthesis methods and to inhomogeneity in particle size distributions [27].

This stimulated our development of nanoparticle synthesis with high-intensity x-ray irradiation, with accurate control over nucleation and growth [1–4]. The approach was successfully applied, for example, to polyethylene glycol (PEG)–Au and core-shelled Au–Ni nanoparticles. The advantages were multiple and clear: excellent colloidal stability, reproducibility, accurate size control, and a one-pot process that makes it simpler to achieve biocompatibility.

So far, this method could not be extended to nanorods in spite of our extensive efforts. We finally identified an effective solution for this problem as described here. The solution provides reproducible control of the aspect ratio while preserving other positive aspects such as a narrow size range and good biocompatibility.

Basically, our approach requires tuning the irradiation intensity at different levels for the two stages of the nanorod production process (seed creation and nanorod growth). For the seed creation, a higher intensity is needed. On the contrary, a high irradiation intensity was found to be counterproductive for the subsequent nanorod growth.

In addition to the details of the synthesis method, here we also describe the extensive characterization of the products. The nanorod solutions were analyzed with ultraviolet–visible (UV–vis) spectroscopy, optical microscopy and transmission x-ray microscopy. Cellular uptake was studied with inductively coupled plasma mass spectrometry (ICP-MS) and biocompatibility was assessed with cell viability assays.

2. Experimental procedure

2.1. Materials

Hexadecyltrimethylammonium bromide (CTAB), silver nitrate (AgNO_3), L-ascorbic acid, 3-(4,5-dimethylthiazol-2-yl)-2,5-diphenyltetrazolium bromide (MTT), $10 \times$ phosphate buffered

saline (PBS), trypsin and hydrogen tetrachloroaurate trihydrate ($\text{HAuCl}_4 \cdot 3\text{H}_2\text{O}$) were purchased from Aldrich Sigma (St. Louis, MO). Glutaraldehyde (25%) and sodium dodecyl sulfate (SDS) were purchased from JTBaker (Phillipsburg, NJ). High-sugar Dulbecco's modified Eagle's medium (DMEM), penicillin, streptomycin, and fetal bovine serum (FBS) were purchased from Invitrogen (Paisley, UK). All solvents and reagents were of analytical grade and used without further purification. Human cervical cancer cells (HeLa cells) were purchased from ATCC (Rockville, MD).

2.2. X-ray synthesis of gold nanorods

As already mentioned, nanorods were produced in a two-step process: the first step was the irradiation-induced formation of initial seeds and the second the nanorod growth from seeds. Such a growth was obtained either by chemical reduction synthesis or by irradiation-induced reduction synthesis.

Gold seeds were synthesized from a 10 ml solution (double distilled deionized Milli-Q water) containing 0.1 M CTAB and 0.00025 M $\text{HAuCl}_4 \cdot 3\text{H}_2\text{O}$ sealed in a 15 ml plastic vial placed upright in the specimen stage and bombarded with x-rays. During irradiation, the solution was at room temperature and there was no stirring. The irradiation time was 5 min at the BL01A beam line of the NSRRC (National Synchrotron Radiation Research Center) with an electron storage ring current of either 300 or 360 mA. Transmission electron microscopy, Fourier transform infrared and UV–vis spectroscopy did not reveal any difference between the seeds synthesized with these two storage ring currents. A detailed description of the beamline was reported elsewhere [28]. The photon energy distribution was centered between 10 and 15 keV and the dose rate was $5.1 \pm 0.9 \text{ kGy s}^{-1}$ as determined by a Fricke dosimeter with an estimated G value of 13.

To prepare the growth solution, we used two methods. The first method was based on the standard chemical reduction synthesis approach: 5 ml of 0.2 M CTAB were mixed with five different volumes (0.05, 0.1, 0.15, 0.2, 0.25 ml) of 0.004 M AgNO_3 . Then, 5.0 ml of 1.0 mM $\text{HAuCl}_4 \cdot 3\text{H}_2\text{O}$ and 70 μl of 0.0788 M ascorbic acid as the reductant were added after gently mixing the solution. Finally, 12 μl of the seed solution was added to the growth solution at 28 °C and left undisturbed for 24 h.

The second method used attenuated x-ray irradiation to replace the ascorbic acid as the reduction agent. The growth solution was prepared in the same way as for the chemical reduction method but without adding ascorbic acid. Twelve microliters of gold seed solution synthesized by x-ray irradiation were added to the growth solution. A 16 μm aluminum sheet was used to attenuate the x-ray intensity for the growth phase. The resulting intensity was much lower than the unattenuated storage ring emission for a 300 mA beam current. The solution was irradiated for 60 min and the color of the solution gradually changed. After irradiation, the solution was left undisturbed for 24 h at 28 °C. Excess CTAB was removed to reduce toxicity by several centrifugation cycles. This involved centrifuging 1 ml of the rod solution in a 1.5 ml microcentrifuge tube at 7000 g for 10 min. The pellet was

resuspended in 1 ml of deionized water and centrifuged again. The gold nanorods were then again resuspended in 900 μl water; at this point, the CTAB concentration was ≈ 0.01 M.

2.3. Characterization of gold nanorods

UV-vis light absorption spectra were taken with a Shimadzu UV-160 spectrometer with a 1 cm quartz cuvette. Transmission electron microscope (TEM) images of the gold nanorods synthesized by x-ray irradiation were compared to those of nanorods prepared by chemical methods. The TEM analysis was performed with a JEOL JEM 2010 F field emission gun transmission electron microscope (FEG-TEM) operating at 200 kV. The samples for TEM measurements were prepared by placing droplets of nanoparticle-containing solution on carbon-coated Cu grids and allowed to dry at room atmosphere.

2.4. Cell culture and treatments

HeLa cells were cultured in DMEM, supplemented with 10% fetal bovine serum, 100 U ml^{-1} penicillin and 100 $\mu\text{g ml}^{-1}$ streptomycin at 37 °C in a humidified atmosphere with 5% CO_2/air . For the MTT assays, the cells were seeded in 96-well plates (Corning, Lowell, USA) at a density of 3.0×10^3 cells/well in 200 μl culture medium. For the other tests, the cells were seeded in 6-well plates (Corning, Lowell, USA) at a density of 3.0×10^6 cells/well in 4 ml of culture medium. All cells were exposed to gold nanorods after 60% confluence. Gold nanorods were freshly dispersed in the cell culture medium and diluted to 2 $\mu\text{g ml}^{-1}$. Microscopy examination was performed after 6 h. Culture media without gold nanorods served as the control in each experiment.

2.5. Analysis of cell viability

Cell viability was measured by using the MTT assay [29]. Cells in the 96-well plates were treated for 48 h with culture media containing gold nanorods of different shapes. Twenty microliters of a 5 mg ml^{-1} solution of MTT in 0.01 M PBS were added to each well and the plates were incubated at 37 °C in 5% CO_2/air for 4 h. The medium was then carefully removed. The purple products were dissolved in SDS. Absorbance was measured at 570 nm using a microplate reader (Bio-Rad 680, Bio-Rad Co., Hercules, USA). All experiments were repeated three times and the data are represented as the mean \pm SE.

2.6. ICP-MS analysis

HeLa cells were exposed to a 2 $\mu\text{g ml}^{-1}$ gold nanorod solution synthesized by x-ray irradiation at 300 mA in a cell culture medium for 0, 1, 2, 4, 6, and 12 h to determine the cell saturation of nanoparticles. To compare the uptake of nanorods of different aspect ratios, the cells were exposed to nanoparticles for a constant time of 6 h. After incubation, the culture medium was removed and washed with PBS three times, the cells were treated with trypsin solution (2%) for 30 min at 37 °C and the subsequent cell dispersion was further sonicated for 2 h in a hot water bath to completely disrupt the

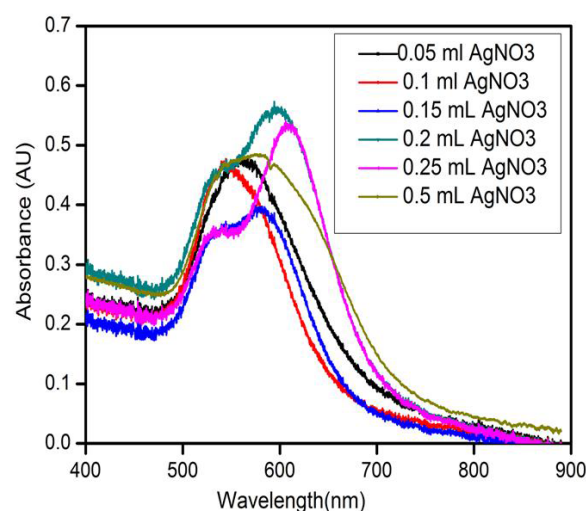


Figure 1. UV-visible spectra of gold nanorods grown by chemical reduction from seeds synthesized by synchrotron x-ray irradiation with a storage ring current of 300 mA, for different silver nitrate concentrations in the precursor solution.

cell membranes. Finally, the gold nanoparticles were dissolved by successively adding 0.3 ml HCl (37% by vol.) and 0.1 ml HNO_3 (70% by vol.). The solution was diluted with deionized water until the HCl concentration reached 2% (vol.). The concentration of gold was determined by ICP-MS (ICP-MS 7500 CS, Agilent Technologies, USA).

2.7. X-ray microscopy analysis

Transmission x-ray microscopy (TXM) was performed at the 32-ID beamline of the Advanced Photon Source (APS), Argonne National Laboratory and the 01B beamline of NSRRC. The cells were cultured on 100 nm-thick silicon nitride support films, rinsed in 0.1 M phosphate-buffered saline (PBS). Cells were fixed with 2.5% glutaraldehyde in 0.1 M PBS and washed. They were then dehydrated using a graded ethanol series (30%, 50%, 70%, 90% and 100%, for 30 min each). The transmitted and tomography images were acquired by TXM. To obtain three-dimensional reconstructions by x-ray nanotomography, 71 sequential projection images were collected from -70° to $+70^\circ$ in 2° intervals at 8.0 keV.

3. Results and discussion

3.1. Synthesis and characterization of gold nanorods produced by x-ray irradiation

The first part of the tests concerns the characterization of the seeds produced by different intensities of x-ray irradiation and different silver nitrate concentrations in the precursor solution. Figures 1 and 2 show typical results: UV-vis spectra of nanorods grown by chemical reduction starting from seeds produced by x-ray irradiation. The two figures differ from each other by way of the irradiation intensity, corresponding to different currents in the electron storage ring. For figure 1, the ring current was 300 mA whereas for figure 2 it was

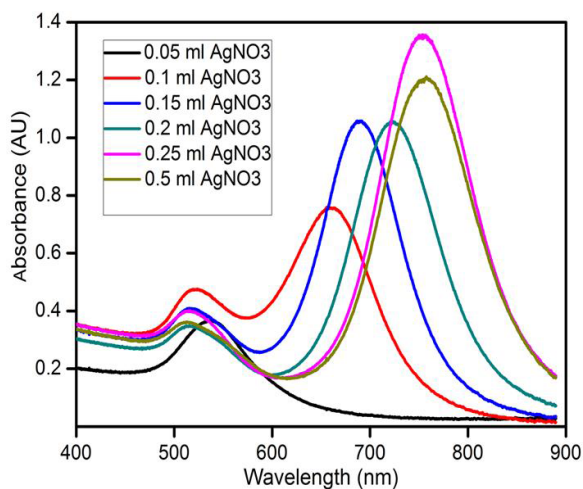


Figure 2. UV-visible spectra similar to figure 1 but for a storage ring current of 360 mA.

360 mA. In each case, spectra are reported for different AgNO_3 concentrations.

Two different absorption peaks are visible in each spectrum, corresponding to the longitudinal and transverse surface plasmon modes. For practical applications, it is desirable to have a longitudinal plasmon peak shifted as much as possible towards the infrared. Both figures 1 and 2 show that this peak position depends on the AgNO_3 concentration [22]. The optimum result in figure 1 is given by 0.25 ml of AgNO_3 , producing plasmon peaks at 530 and 630 nm, whereas for other AgNO_3 concentrations there is little or no longitudinal plasmon peak, indicating that no large-aspect-ratio nanorods were formed. Even for the optimal case, the shift is limited. Overall, the results in figure 1 are not particularly interesting.

Figure 2 shows instead a successful result. Both peaks are visible, indicating nanorod formation, and the longitudinal plasmon peak is shifted well towards the infrared. The figure shows that AgNO_3 in suitable concentration is required to obtain the nanorods. The role of AgNO_3 in the nanorod synthesis was proposed and experimentally investigated by previous studies [18]. Silver ions are adsorbed on the gold

nanoparticle surface in the form of AgBr , inhibit the growth and stabilize the surface of the nanorods. In our present work, we confirmed that the presence and concentration of AgNO_3 is crucial to the growth [30].

Also note that both figures 1 and 2 correspond to tests conducted in the presence of CTAB both in the seed-production phase and in the nanorod-growth phase. With no CTAB in both phases, no nanorods were obtained. CTAB in this process functions as a soft rodlike micellar template that alters the otherwise isotropic growth of Au on seeds and directs the growth by blocking the long-axis crystal faces, promoting metal growth on the short-axis faces and producing nanorods [30]. This leads to material addition along the [110] common axis on {111} faces that do not contain the CTA^+ headgroups. Our present experiments confirmed that without CTAB only spherical and/or cuboid shape nanoparticles are synthesized.

The UV-vis results of figures 1 and 2 are corroborated by the TEM images of figures 3(A) and (B), corresponding again to chemically grown nanorods from seeds produced by irradiation at 300 and 360 mA. In both cases, the AgNO_3 concentration was 4×10^{-4} M. The average nanorod aspect ratio for 300 mA (figure 3(A)) is small, ~ 1.4 , with an average diameter ≈ 50 nm. But at 360 mA (figure 3(B)) the average aspect ratio is ~ 5 , corresponding to a length of ~ 70 nm and a diameter of ~ 14 nm. Furthermore, the nanorod size and shape is quite uniform. Specifically, a much smaller proportion ($< 1\%$) of cuboid particles exists compared to figure 3(A). The reason that a small percentage of cuboid particles is formed for 360 mA irradiation is not entirely clear, but we believe that a more uniform chemical reaction induced by a high penetration radiation can lead to a more uniform growth morphology than conventional solution chemistry methods.

In summary, a suitably high irradiation intensity in the seed creation phase makes it possible to obtain final nanorods with a uniform geometric distribution and high aspect ratio. The results from different ring currents in figures 1–3 were indeed corroborated by complementary tests in which the irradiation intensity was tuned by attenuating the x-ray beam at a given ring current.

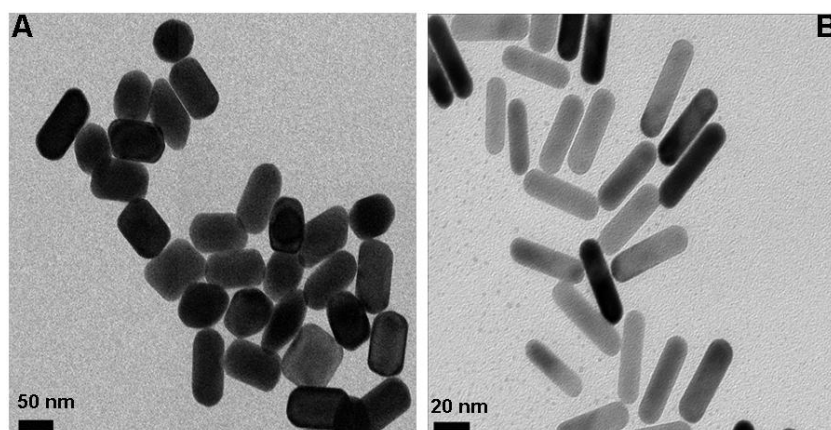


Figure 3. TEM images of gold nanorods, corresponding to those of figures 1 and 2, chemically grown from seeds created by synchrotron x-ray irradiation with a storage ring current of (A) 300 and (B) 360 mA.

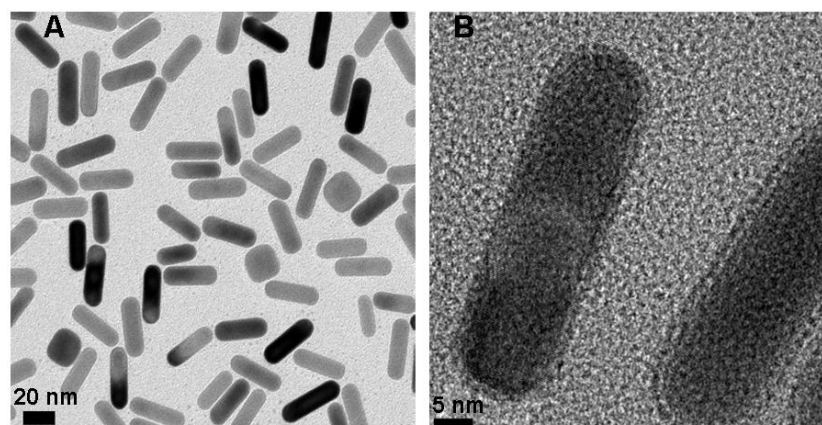


Figure 4. TEM images of gold nanorods grown from seeds created by x-ray irradiation in the presence of 0.1 mM AgNO₃. Contrary to figures 1–3, in this case the nanorod growth was obtained from additional x-ray irradiation at reduced intensity, rather than by chemical reduction.

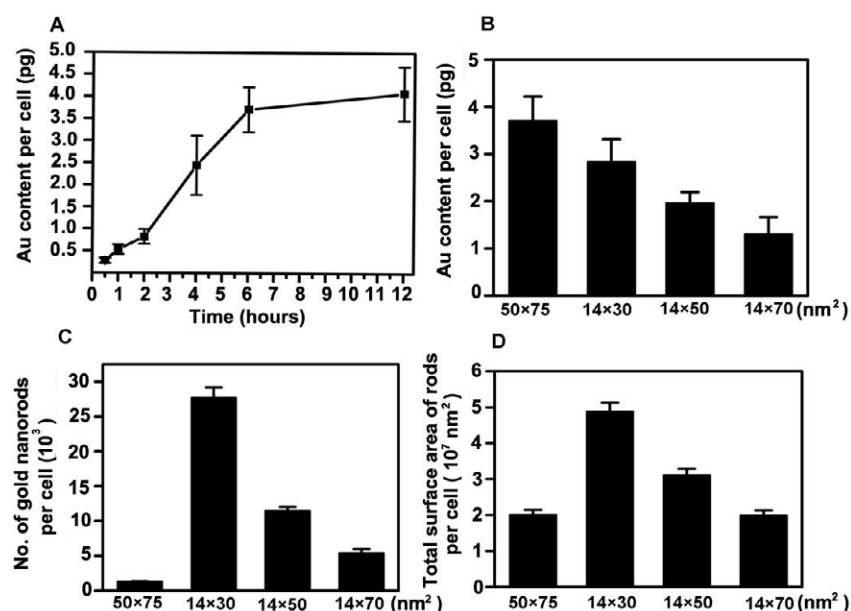


Figure 5. (A) Gold concentrations versus time measured by ICP-MS in HeLa cells incubated with Au nanorods similar to those of figures 1–3. (B) The Au quantity per cell is affected by the nanoparticle aspect ratio. (C) An estimate of the number of nanoparticles per cell based on the data in (B). (D) An estimate of the total surface area of nanoparticles per cell. A crude calculation (assuming cubes and cylinders) was performed to visually compare how the quantity of gold per cell could reflect numbers of nanoparticles and total surface area of nanoparticles per cell (figures (C) and (D)).

A pertinent question at this point is: can the nanorods from the optimized seeds also be obtained by irradiation rather than by chemical reduction? All our initial tests seemed to point to a negative response: no nanorods were produced by irradiation. Eventually, however, we found the key of the problem.

In fact, high-intensity irradiation, which is positive for the seed creation, becomes detrimental for the nanorod growth. Tests with a 300 mA ring current did produce nanorods after the irradiating beam was attenuated by two orders of magnitude. Typical results are shown by the TEM micrographs of figures 4(A) and (B). This success is essentially empirical: although we can speculate on its causes, these must still be clarified by additional tests.

3.2. Cellular uptake and distribution

In order to test the possible use in nanomedicine of nanorods produced by our approach, we performed cell uptake and biocompatibility tests. Note that CTAB is an antiseptic, toxic to most cells. However, in our conditions ($2 \mu\text{g ml}^{-1}$ gold nanorods in cell culture medium), the very low concentration of CTAB did not exhibit cytotoxicity toward HeLa cells after 48 h, based on MTT assays (data not shown).

The uptake by HeLa cells of nanorods synthesized by x-ray irradiation (from seeds also obtained by x-ray irradiation) was determined by ICP-MS. As seen in figure 5(A), the cellular Au content of gold nanorods with an aspect ratio of

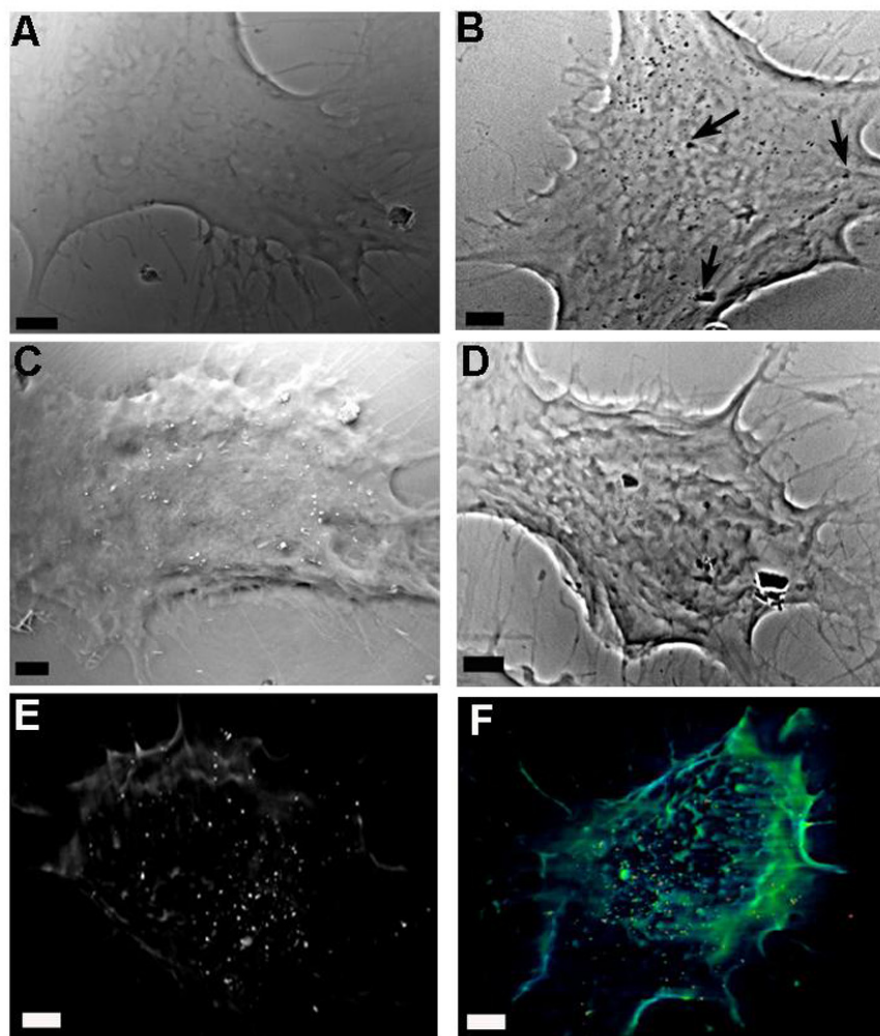


Figure 6. Transmitted x-ray microscope images of gold nanorods, similar to those of figures 1–3 and 5 (seeds obtained by x-ray irradiation, at 300 and 360 mA), and HeLa cells after 6 h of co-culture. (A) A normal HeLa cell (control image). (B) A HeLa cell with nanorods grown at 300 mA. Those large aggregates marked by arrows appeared (by 3D reconstruction) adhere to the surface rather than being uptaken by the cells. (C) and (D) A HeLa cell with nanorods grown at 360 mA in HeLa cells. The white dots in (C) were due to contrast reversal by adjusting the Zernike contrast. (E) and (F) Images from three-dimensional tomography reconstruction (with different gray scale for better visualization of the nanoparticle and the whole cell) confirming the internalization of nanorods by a HeLa cell. Scale bar = 2 μm .

1.4 gradually increased with the incubation time, reaching a plateau at ~ 6 h. Thus, 6 h was used as the incubation time for subsequent intracellular uptake assays and for comparisons of the cellular uptake of nanorods synthesized by different methods.

Cellular Au uptake in the form of nanoparticles strongly depends on the size and shape. In one example, the maximum uptake occurred for spherical Au nanoparticles of 50 nm size, while smaller uptake was observed for rod-shaped Au nanoparticles [31]. The results in figure 5(B) suggest a similar conclusion in that the largest uptake was for cuboid particles. Homogeneous and reproducible synthesis is therefore important for practical applications and for controlling the nanorod behavior.

At first glance, the applicability of nanorods for nanomedicine appears diminished since the cellular Au uptake is significantly limited compared to cuboids. However,

what is of greater importance here could be the nanoparticle numbers and their total surface area rather than the absolute amount of Au uptake. In the case of cuboid nanoparticles, figure 5(B) could be misleading since the corresponding number of nanoparticles internalized is actually small, due to the large amount of Au per nanoparticle of this type. A crude calculation (assuming cubes and cylinders) reveals visually that the numbers of nanoparticles, figure 5(C), and total surface area of nanoparticles per cell, figure 5(D), could be interpreted quite differently as that shown in figure 5(B).

In essence, these cellular uptake results stress that shape and size tailoring, as allowed by our methods, are important to optimize the products for different objectives. For example, for radiation enhancement (i.e. maximizing the absorption of radiation energy) for therapeutic effects, the optimal shape can be different than for drug or gene delivery, for which surface area plays an important role.

The internalization and distribution of nanorods at sub-cellular level was investigated by taking high-resolution (17 nm) transmission x-ray microscope (TXM) images of HeLa cells [32]. Figure 6(A) shows an example of such image of a HeLa cell where the cell membrane and filopodia are clearly observed. Note that no staining was applied and the sub-cellular organs, such as the cell nucleus and mitochondria, are not clearly visible. Cellular incorporation of the nanorods (with seeds grown at 300 mA) after 6 h of co-culture is nevertheless clear in figure 6(B). These micrographs revealed that some rods (marked with arrows) appear to adhere to the cell surface rather than being internalized. Note that ICP-MS cannot distinguish between internalized and surface-absorbed nanorods.

Nanorods synthesized from seeds grown by x-ray irradiation at 360 mA were also imaged after co-culturing with HeLa cells for 6 h and found to be incorporated by endocytosis (figures 6(C) and (D)). The white dots in figure 6(C) were due to contrast reversal by adjusting the Zernike contrast. This is an interesting feature of the x-ray optical setup allowing identification of objects of different alteration of the phase. In this case, we can confirm by comparison that those are Au. Tomography reconstruction in three dimensions [32–34] (figures 6(E) and (F)) revealed that x-ray synthesized nanorods in HeLa cells are mostly located in the cytoplasm. The reconstruction is based on standard filter back projection algorithm after each individual projection image (a total of 70 of them from -70 to 70° with respect to the incident beam direction) is aligned to remove the error from imperfect mechanical rotation movement. This alignment is performed by following sharp features, such as the Au nanorods in the cells, with respect to the expected position in rotation. After reconstruction, a 3D model is constructed and images such as 6(E) and (F) are generated from the model at a selected viewing position. The location of each individual nanorod can be clearly identified with respect to the cell boundary in 3D.

Our present result, however, does not fully clarify the underlying growth mechanism at the molecular level. Note, however, that the ionization and excitation of the solvent due to the irradiation leads to the formation of radiolytic molecular and radical species, such as solvated electrons, e_{aq}^- , and hydrogen atoms H^\bullet [35]. These have strong redox potentials, capable of reducing metal ions to lower valences and finally to metal atoms. It is probable that in our irradiation synthesis these species are responsible for reducing metallic ions to their atomic form. It was previously demonstrated [36] that the reduction of Au from a pure precursor in aqueous solution can be completely achieved by x-ray irradiation alone without addition of any reductant. The chemicals added in the synthesis treated here, therefore, are not likely responsible for the reduction. Both $AgNO_3$ and CTAB are required and their respective roles were previously investigated; their presence restricts the otherwise isotropic growth to specific crystal faces resulting in large-aspect-ratio rod-shaped nanoparticles. The reason that both are required, however, is not entirely clear. We also confirmed that the growth in a preferential direction is linked to a slow reaction rate, requiring either weak reductants or low-intensity irradiation.

4. Conclusions

Au seeds for the growth of nanorods were synthesized using synchrotron x-ray irradiation and the ability to generate high aspect ratio nanorods was improved by increasing the irradiation intensity. The final nanorods had a uniform and tunable aspect ratio with high colloidal stability. The tunable aspect ratio makes it possible to optimize the nanorods for maximizing Au cellular internalization or for red-shifted absorption.

After the production of seeds, the growth of nanorods can be obtained either by chemical reduction or again by x-ray irradiation. The second process is feasible only after drastic attenuation of the irradiation intensity. Although still to be clarified, this second procedure opens interesting possibilities for the production of biocompatible nanorods.

Acknowledgments

Research supported by the National Science and Technology Program for Nanoscience and Nanotechnology, the Thematic Research Project of Academia Sinica, the Biomedical Nano-Imaging Core Facility at National Synchrotron Radiation Research Center (Taiwan), the Fonds National Suisse pour la Recherche Scientifique and by the Center for Biomedical Imaging (CIBM, supported by the Louis-Jeantet and Leenards foundations). The Advanced Photon Source was supported by the US Department of Energy, Office of Science, Office of Basic Energy Sciences, under Contract No. DE-AC02-06CH11357.

References

- [1] Wang C-H, Liu C-R, Wang C-L, Hua T-E, Lee K H and Hwu Y-K 2008 Optimizing the size and surface properties of polyethylene glycol (PEG)-gold nanoparticles by intense x-ray irradiation *J. Phys. D: Appl. Phys.* **41** 195301
- [2] Wang C-H et al 2007 Aqueous gold nanosols stabilized by electrostatic protection generated by x-ray irradiation assisted radical reduction *Mater. Chem. Phys.* **106** 323
- [3] Liu C-J et al 2008 Enhanced x-ray irradiation-induced cancer cell damage by gold nanoparticles treated by a new synthesis method of polyethylene glycol modification *Nanotechnology* **29** 295104
- [4] Kim C-C et al 2006 X-ray synthesis of nickel-gold composite nanoparticles *Mater. Chem. Phys.* **100** 292
- [5] Sun Y and Xia Y 2002 Shape-controlled synthesis of gold and silver nanoparticles *Science* **298** 2176
- [6] Huang X, El-Sayed I H, Qian W and El-Sayed M A 2006 Cancer cell imaging and photothermal therapy in the near-infrared region by using gold nanorods *J. Am. Chem. Soc.* **128** 2115
- [7] Tong L, Wei Q, Wei A and Cheng J-X 2009 Gold nanorods as contrast agents for biological imaging: optical properties, surface conjugation and photothermal effects *Photochem. Photobiol.* **85** 21
- [8] Tong L and Cheng J X 2009 Gold nanorod-mediated photothermal lysis induces apoptosis of macrophages via damage of mitochondria *Nanomedicine* **4** 265
- [9] Skrabalak S E, Chen J, Sun Y, Lu X, Au L, Copley C M and Xia Y 2008 Gold nanocages: synthesis, properties, and applications *Acc. Chem. Res.* **41** 1587

- [10] Pissuwan D, Valenzuela S M, Miller C M and Cortie M B 2007 A golden bullet? Selective targeting of toxoplasma gondii tachyzoites using antibody-functionalized gold nanorods *Nano Lett.* **7** 3808
- [11] Norman R S, Stone J W, Gole A, Murphy C J and Sabo-Attwood T L 2007 Targeted photothermal lysis of the pathogenic bacteria, pseudomonas aeruginosa, with gold nanorods *Nano Lett.* **8** 302
- [12] Huang X, Jain P K, El-Sayed I H and El-Sayed M A 2007 Gold nanoparticles: interesting optical properties and recent applications in cancer diagnostics and therapy *Nanomedicine* **2** 681
- [13] Durr N J, Larson T, Smith D K, Korgel B A, Sokolov K and Ben-Yakar A 2007 Two-photon luminescence imaging of cancer cells using molecularly targeted gold nanorods *Nano Lett.* **7** 941
- [14] Yu C and Irudayaraj J 2006 Multiplex biosensor using gold nanorods *Anal. Chem.* **79** 572
- [15] Chen C-C, Lin Y-P, Wang C-W, Tzeng H-C, Wu C-H, Chen Y-C, Chen C-P, Chen L-C and Wu Y-C 2006 DNA-oligo nanorod conjugates for remote control of localized gene expression by near infrared irradiation *J. Am. Chem. Soc.* **128** 3709
- [16] van der Zande B M I, Bohmer M R, Fokkink L G J and Schonenberger C 1997 Aqueous gold sols of rod-shaped particles *J. Phys. Chem. B* **101** 852
- [17] Kim F, Song J H and Yang P 2002 Photochemical synthesis of gold nanorods *J. Am. Chem. Soc.* **124** 14316
- [18] Placido T, Comparelli R, Giannici F, Cozzoli P D, Capitani G, Striccoli M, Agostiano A and Curri M L 2009 Photochemical synthesis of water-soluble gold nanorods: the role of silver in assisting anisotropic growth *Chem. Mater.* **21** 4192
- [19] Yu Y Y, Chang S-S, Lee C-L and Wang C R C 1997 Gold nanorods: electrochemical synthesis and optical properties *J. Phys. Chem. B* **101** 6661
- [20] Sau T K and Murphy C J 2004 Seeded high yield synthesis of short Au nanorods in aqueous solution *Langmuir* **20** 6414
- [21] Jana N R, Gearheart L and Murphy C J 2001 Seed-mediated growth approach for shape-controlled synthesis of spheroidal and rod-like gold nanoparticles using a surfactant template *Adv. Mater.* **13** 1389
- [22] Nikoobakht B and El-Sayed M A 2003 Preparation and growth mechanism of gold nanorods (NRS) using seed-mediated growth method *Chem. Mater.* **15** 1957
- [23] Zijlstra P, Bullen C, Chon J W M and Gu M 2006 High-temperature seedless synthesis of gold nanorods *J. Phys. Chem. B* **110** 19315
- [24] Biswal J, Ramnani S P, Tewari R, Dey G K and Sabharwal S 2010 Short aspect ratio gold nanorods prepared using gamma radiation in the presence of cetyltrimethyl ammonium bromide (CTAB) as a directing agent *Radiat. Phys. Chem.* **79** 441
- [25] Seino S, Kinoshita T, Nakagawa T, Kojima T, Taniguchi R, Okuda S and Yamamoto T 2008 Radiation induced synthesis of gold/iron-oxide composite nanoparticles using high-energy electron beam *J. Nanopart. Res.* **10** 1071
- [26] Ma Q, Moldovan N, Mancini D C and Rosenberg R A 2000 Synchrotron-radiation-induced, selective-area deposition of gold on polyimide from solution *Appl. Phys. Lett.* **76** 2014
- [27] Karadas F, Ertas G, Ozkaraoglu E and Suzer S 2004 X-ray-induced production of gold nanoparticles on a SiO₂/Si system and in a poly(methyl methacrylate) matrix *Langmuir* **21** 437
- [28] Hsu P-C, Wang C-H, Yang T-Y, Hwu Y-K, Lin C-S, Chen C-H, Chang L-W, Seol S-K, Je J-H and Margaritondo G 2007 Photosynthesis and structure of electroless Ni-P films by synchrotron x-ray irradiation *J. Vac. Sci. Technol. A* **25** 615
- [29] Mosmann T 1983 Rapid colorimetric assay for cellular growth and survival: application to proliferation and cytotoxicity assays *J. Immunol. Methods* **65** 55
- [30] Murphy C J, Sau T K, Gole A M, Orendorff C J, Gao J, Gou L, Hunyadi S E and Li T 2005 Anisotropic metal nanoparticles: synthesis, assembly, and optical applications *J. Phys. Chem. B* **109** 13857
- [31] Chithrani B D, Ghazani A A and Chan W C W 2006 Determining the size and shape dependence of gold nanoparticle uptake into mammalian cells *Nano Lett.* **6** 662
- [32] Yin G-C, Song Y-F, Tang M-T, Chen F-R, Liang K S, Duewer F W, Feser M, Yun W and Shieh H-P D 2006 30 nm resolution x-ray imaging at 8 keV using third order diffraction of a zone plate lens objective in a transmission microscope *Appl. Phys. Lett.* **89** 221122
- [33] Le Gros M A, McDermott G and Larabell C A 2005 X-ray tomography of whole cells *Curr. Opin. Struct. Biol.* **15** 593
- [34] Larabell C A and Le Gros M A 2004 X-ray tomography generates 3D reconstructions of the yeast, saccharomyces cerevisiae, at 60 nm resolution *Mol. Biol. Cell* **15** 957
- [35] Remita H, Lampre I, Mostafavi M, Balanzat E and Bouffard S 2005 Comparative study of metal clusters induced in aqueous solutions by γ -rays, electron or C⁶⁺ ion beam irradiation *Radiat. Phys. Chem.* **72** 575
- [36] Wang C H, Chien C C, Yu Y L, Liu C J, Lee C F, Chen C H, Hwu Y, Yang C H, Je J H and Margaritondo G 2007 Structural properties of 'naked' gold nanoparticles formed by synchrotron x-ray irradiation *J. Synchrotron Radiat.* **14** 477